Electronic Supplementary Material (ESI) for Inorganic Chemistry Frontiers.

Supporting Information

NiFeCu phosphides with surface reconstruction via topotactic transformation of layered double hydroxides for overall water splitting

Jingmin Ge‡, Shuteng Diao‡, Jiaxing Jin, Yiping Wang, Xuhui Zhao, Fazhi Zhang, Xiaodong Lei**

State Key Laboratory of Chemical Resource Engineering, Beijing University of Chemical Technology, Beijing 100029, China.

E-mail address: wangyiping@buct.edu.cn; leixd@mail.buct.edu.cn

Tel: +86-10-64455357

‡These authors contributed equally

Materials, Electrochemical measurement and Computational Methods

Materials

Nickel (II) nitrate hexahydrate ($Ni(NO_3)_2 \cdot 6H_2O$), Iron (III) nitrate nonahydratenickel ($Fe(NO_3)_3 \cdot 9H_2O$) and copper (II) nitrate hydrate ($Cu(NO_3)_2 \cdot 3H_2O$) were obtained from Aldrich. Ammonium fluoride (NH_4F) was purchased from Macklin. Sodium phosphinate hydrate ($NaH_2PO_2 \cdot H_2O$) came from Beijing Chemical works. nickel foam (NF) with a thickness of 0.5 mm was bought from CST Conscitech. The other chemicals were of analytical grade and were purchased from Sinopharm Chemical Reagents Co.. All chemicals were used without further purification.

Electrochemical measurement

Electrochemical measurements were performed on an electrochemical workstation (CHI 660E, Chenhua, Shanghai) using a three-electrode mode in Ar-saturated 1 $mol \cdot L^{-1}$ KOH aqueous solution. A platinum electrode was used as counter electrode, sliver/sliver chloride (Ag/AgCl) electrode was used as the reference electrode, and the as-fabricated materials were used for the working electrodes. The potentials were converted to the RHE scale using the following Nernst equation: (E(RHE) = E(Ag/AgCl) + 0.059 pH + 0.197). The electrochemical impedance spectroscopy (EIS) tests were performed in the frequency range from 100 kHz to 0.1 Hz at an overpotential of 100 mV. A long-term stability tests were recorded by taking a chronoamperometric curve current density reached 10 $mA \cdot cm^{-2}$. All data were presented without IR-compensation. All the electrochemical tests were tested at room temperature.

Computational Methods

All first-principle calculations were performed by using density functional theory (DFT) in the Cambridge Sequential Total Energy Package (CASTEP) module in

Materials Studio. The exchange-correlation interactions were treated within the generalized gradient approximation of the Perdew-Burke-Ernzerhof (PBE) type. The plane-wave cutoff energy was 400 eV and a k-mesh of 2 ×2 × 1 was adopted to sample the Brillouin zone. The convergence threshold for energy and Hellmann-Feynman forces on each atom were set to 10^{-5} eV and 0.01 eV $Å^{-1}$. Vacuum layers of 25 Å were introduced to minimize interactions between adjacent layers in all supercells.

Gibbs free-energy of the adsorbed species was calculated by the following formula:

$$\Delta G = \Delta E + \Delta ZPE - T\Delta S \quad (1)$$

where ΔE is the adsorption energy of the adsorbed species on the given unit cell, ΔZPE and $T\Delta S$ are the zero-point energy and entropy difference of the adsorbed species in the adsorbed state and the gas phase, respectively. The value of ZPE and TS for the adsorbed species can be calculated from the vibration frequencies, as shown in previous literatures [1, 2].

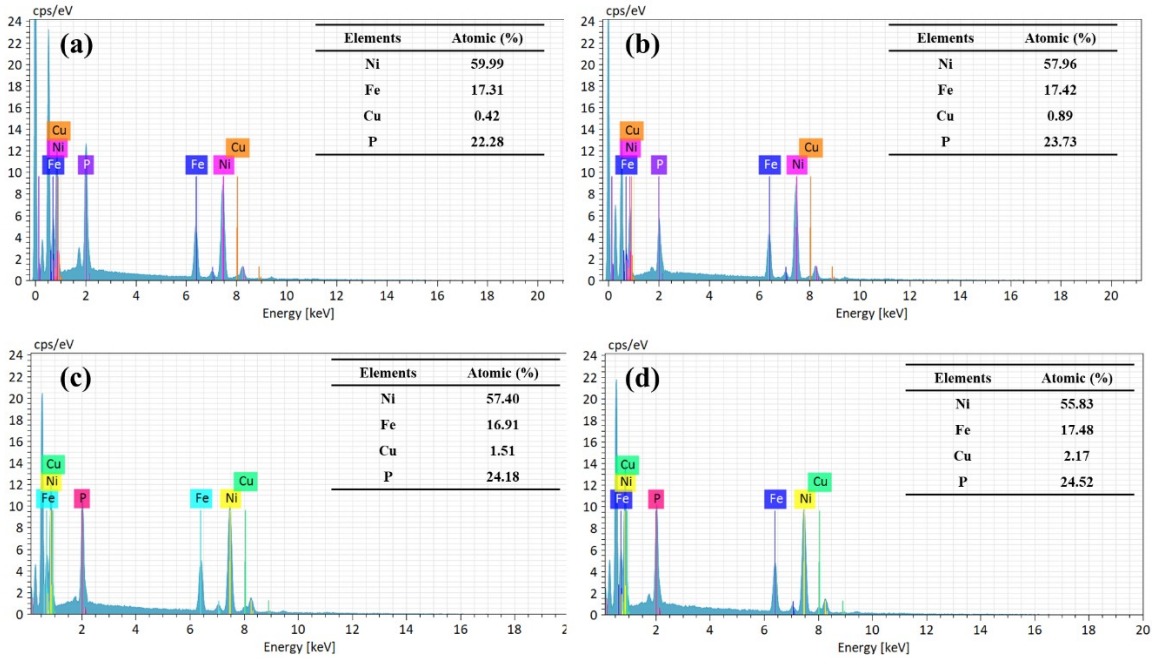

Figure S1. EDS spectra and corresponding element ratios of (a) NiFeCuP-1, (b) NiFeCuP-2, (c) NiFeCuP-3 and (d) NiFeCuP-4.

9 mmol of $Ni(NO_3)_2 \cdot 6H_2O$ and 3 mmol $Fe(NO_3)_3 \cdot 9H_2O$, 39 mmol NH_4F, 86 mmol $CO(NH_2)_2$ and various amounts of $Cu(NO_3)_2 \cdot 3H_2O$ (0.5, 1, 1.5 and 2 mmol) were dissolved in 30 mL of deionized (DI) water, and treated NF (1×3 cm^2) was put into the mixed solution, then hydrothermally reacted for 12 h at 120 ºC. The precursors (NiFeCu-LDH-1, NiFeCu-LDH-2, NiFeCu-LDH-3 and NiFeCu-LDH-4/NF) were obtained after washing and vacuum drying. The precursors were phosphatized *via* $NaH_2PO_2 \cdot H_2O$ under nitrogen. After cooling to the room temperature, NiFeCuP-1, NiFeCuP-2, NiFeCuP-3 and NiFeCuP-4 were obtained, respectively.

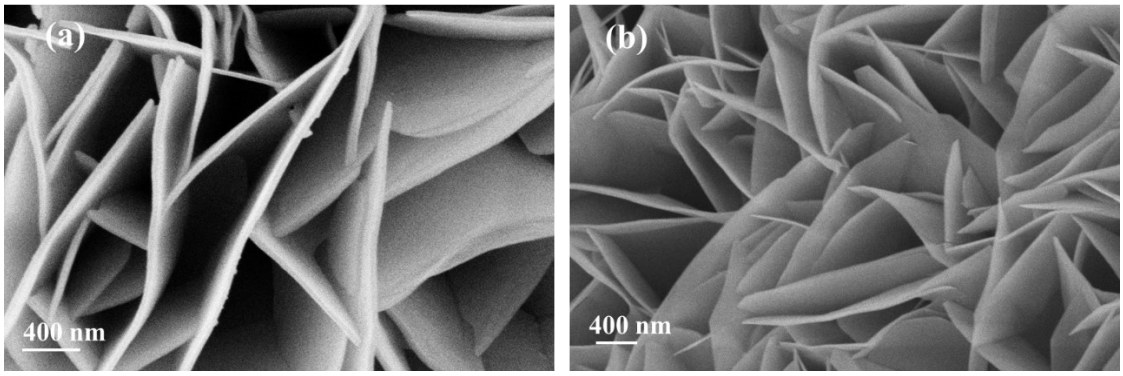

Figure S2. The SEM images of (a) NiFe-LDH and (b) NiFeCu-LDH

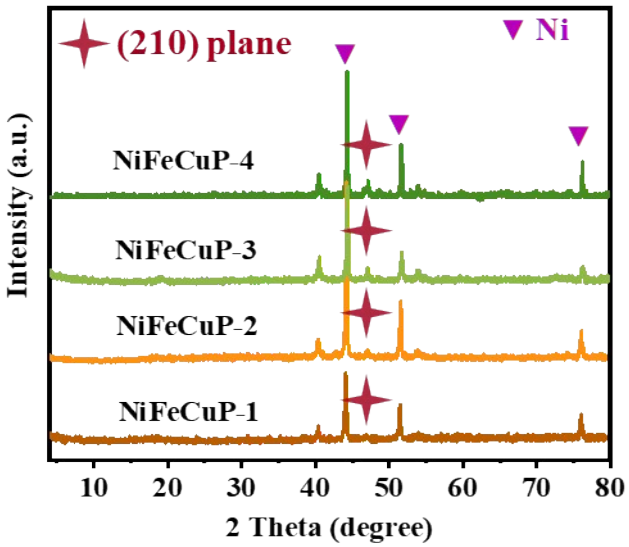

Figure S3. The patterns of NiFeCuP-1, NiFeCuP-2, NiFeCuP-3 and NiFeCuP-4.

The introduction of Cu into NiFeP induces the appearance of (210) crystal plane (the peak at 47.3°). With the increasing amount of Cu introduced into NiFeP, the peak intensity of the peak at 47.3° increases gradually, indicating that the exposure of (210) crystal plane increases gradually.

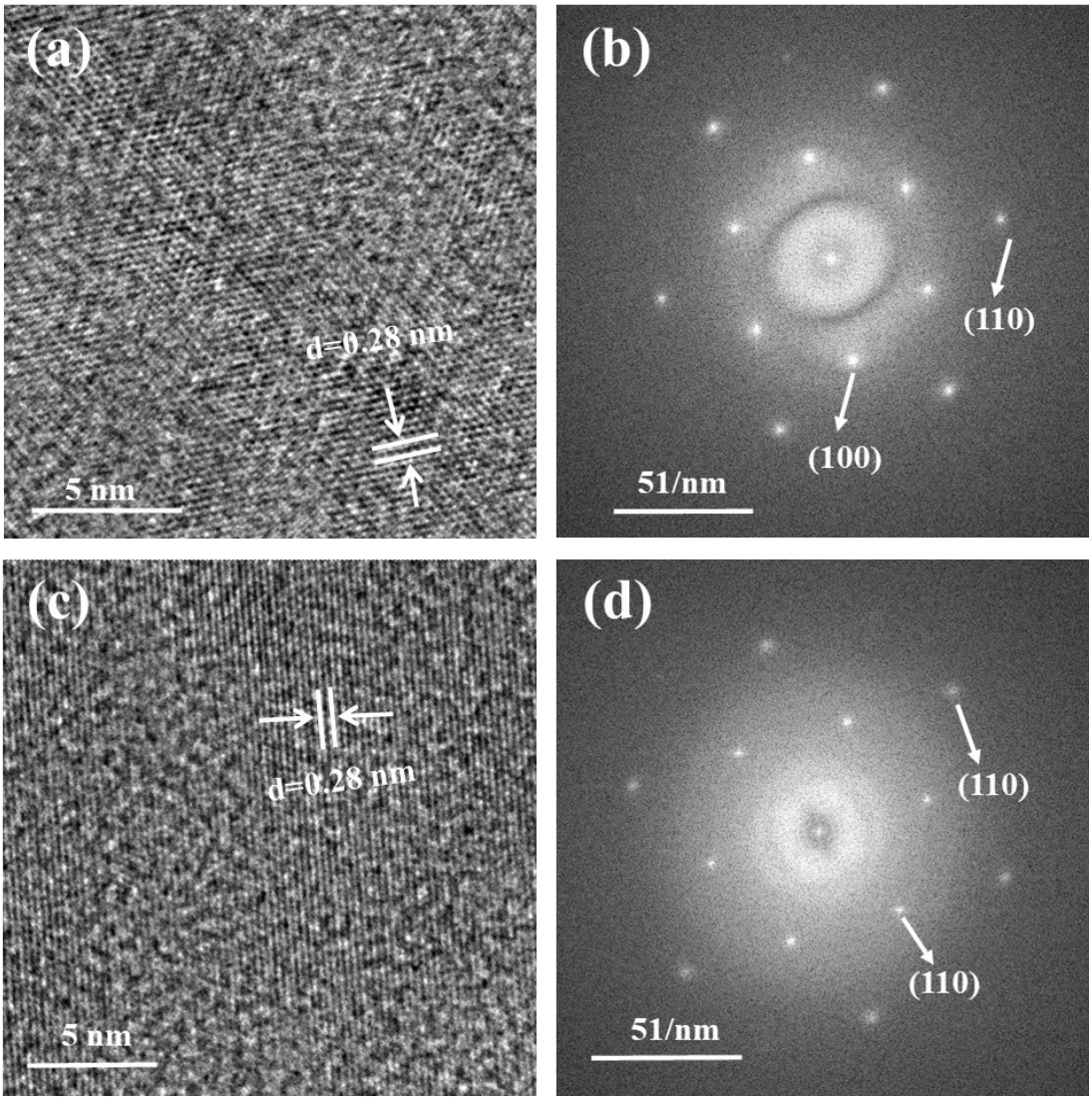

Figure S4. (a) HRTEM image and (b) SAED pattern of NiFe-LDH. (c) HRTEM image and (d) SAED pattern of NiFeCu-LDH.

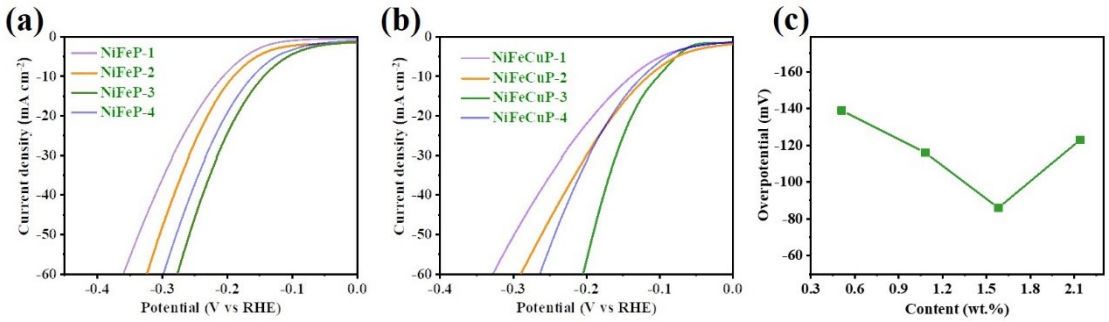

Figure S5. LSV curves of (a) NiFe phosphides and (b) NiFeCu phosphides without IR correct for HER. (c) Plots of the overpotential vs concentration of Cu in NiFeCu phosphides.

By adjusting the addition amount of $Ni(NO_3)_2 \cdot 6H_2O$ and $Fe(NO_3)_3 \cdot 9H_2O$ (The amount of total metal ions was 12 mmol), the samples with different Ni: Fe ratios were prepared. Based on the Ni:Fe ratios (1:1, 2:1, 3:1 and 4:1), they were labeled as NiFeP-1, NiFeP-2, NiFeP-3 and NiFeP-4, respectively. The contents of elements in these samples were tested by ICP-OES (Table S2). In the electrochemical performance tests, NiFeP-3 is found to have the better catalytic performance. For convenience, NiFeP-3 was also labeled as NiFeP in this paper.

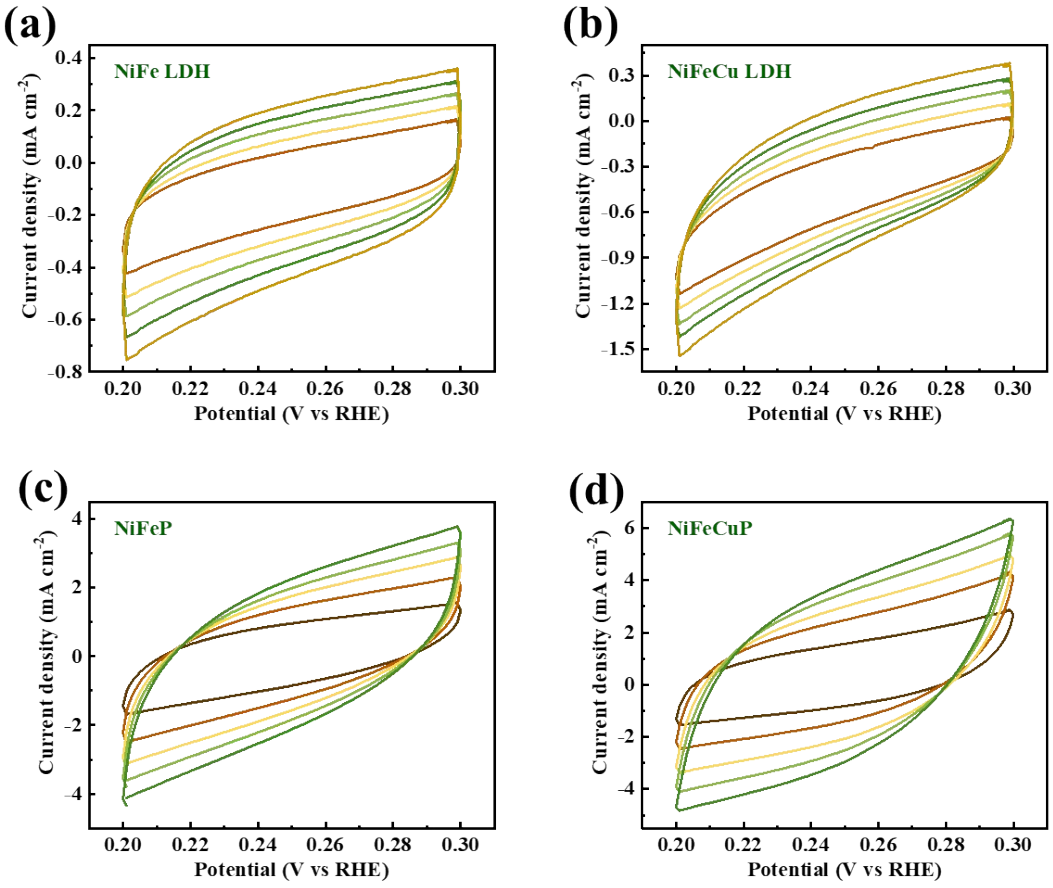

Figure S6. CV curves of (a) NiFe-LDH, (b) NiFeCu-LDH, (c) NiFeP and (d) NiFeCuP at the scan rates of 5, 10, 15, 20, 25 and 30 mV s-1 in 1.0 M KOH.

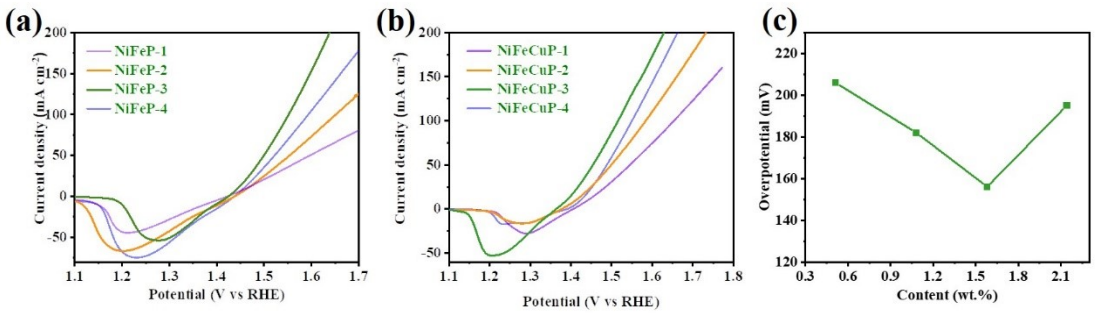

Figure S7. LSV curves of (a) NiFe phosphides and (b) NiFeCu phosphides for OER.

(c) Plots of the overpotential vs concentration of Cu in NiFeCu phosphides.

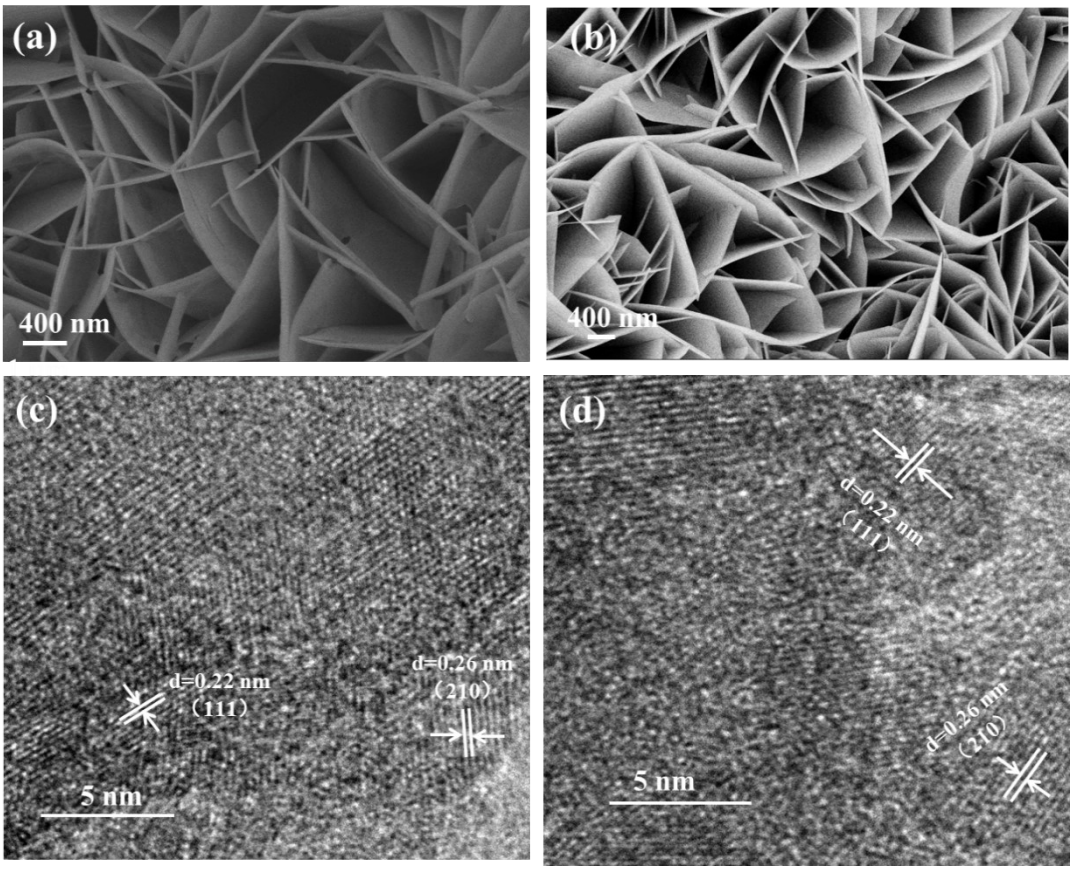

Figure S8. SEM images of NiFeCuP after (a) HER and (b) OER tests. The HRTEM images of NiFeCuP after (c) HER and (d) OER tests.

As shown in Figure S6a and b, the nanosheet arrays do not change significantly after the HER and OER tests, and the nanosheet arrays structure was still clearly visible, indicating that the catalysts have good stability. HRTEM images show that the crystal planes of (111) and (210) are clearly visible after HER and OER tests, which also indicate that the structure of the material remains intact after HER and OER (Figure S6c and d).

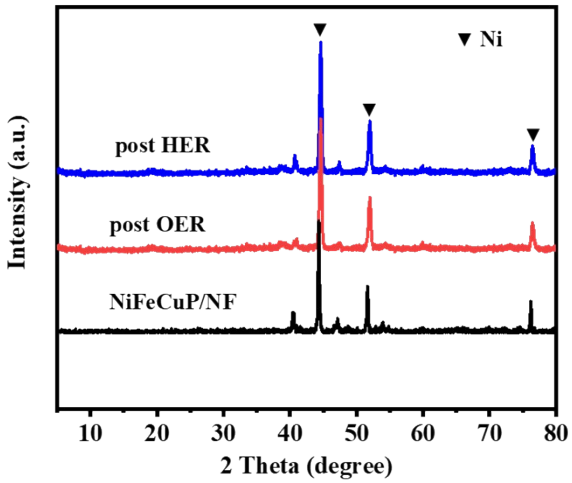

Figure S9. XRD patterns of NiFeCuP after HER and OER tests.

The XRD patterns show that compared with the initial results, the peaks intensity of NiFeCuP/NF do not change significantly after long-term HER and OER tests, indicating that the material has excellent stability.

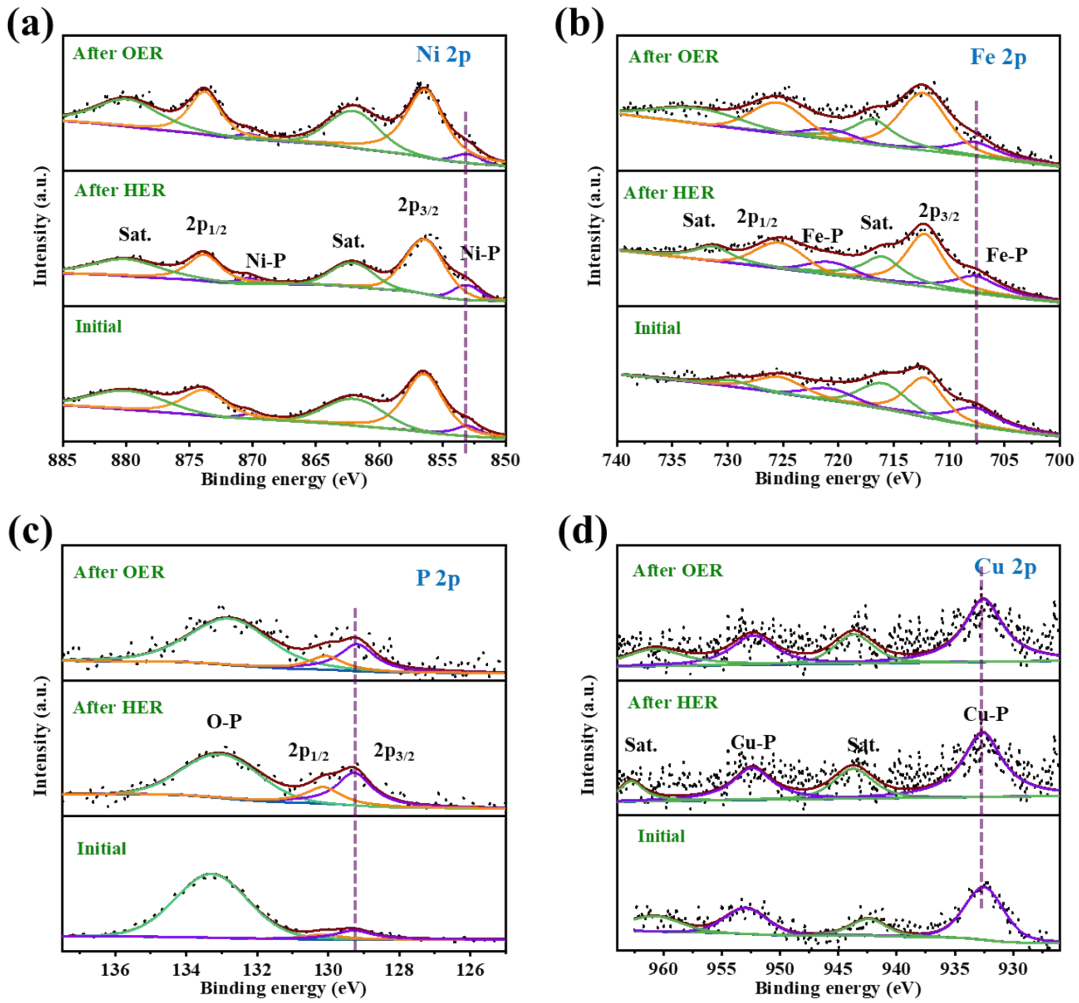

Figure S10. XPS spectra of NiFeCuP and that of after HER and OER tests.

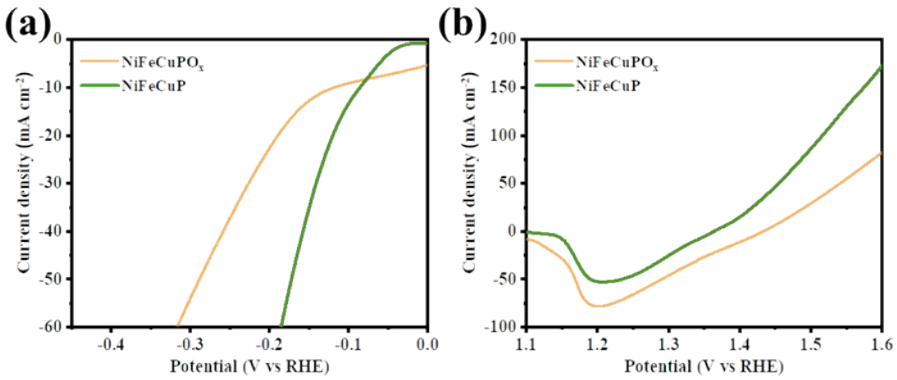

Figure S11. The LSV curves of NiFeCuP and NiFeCuPOx

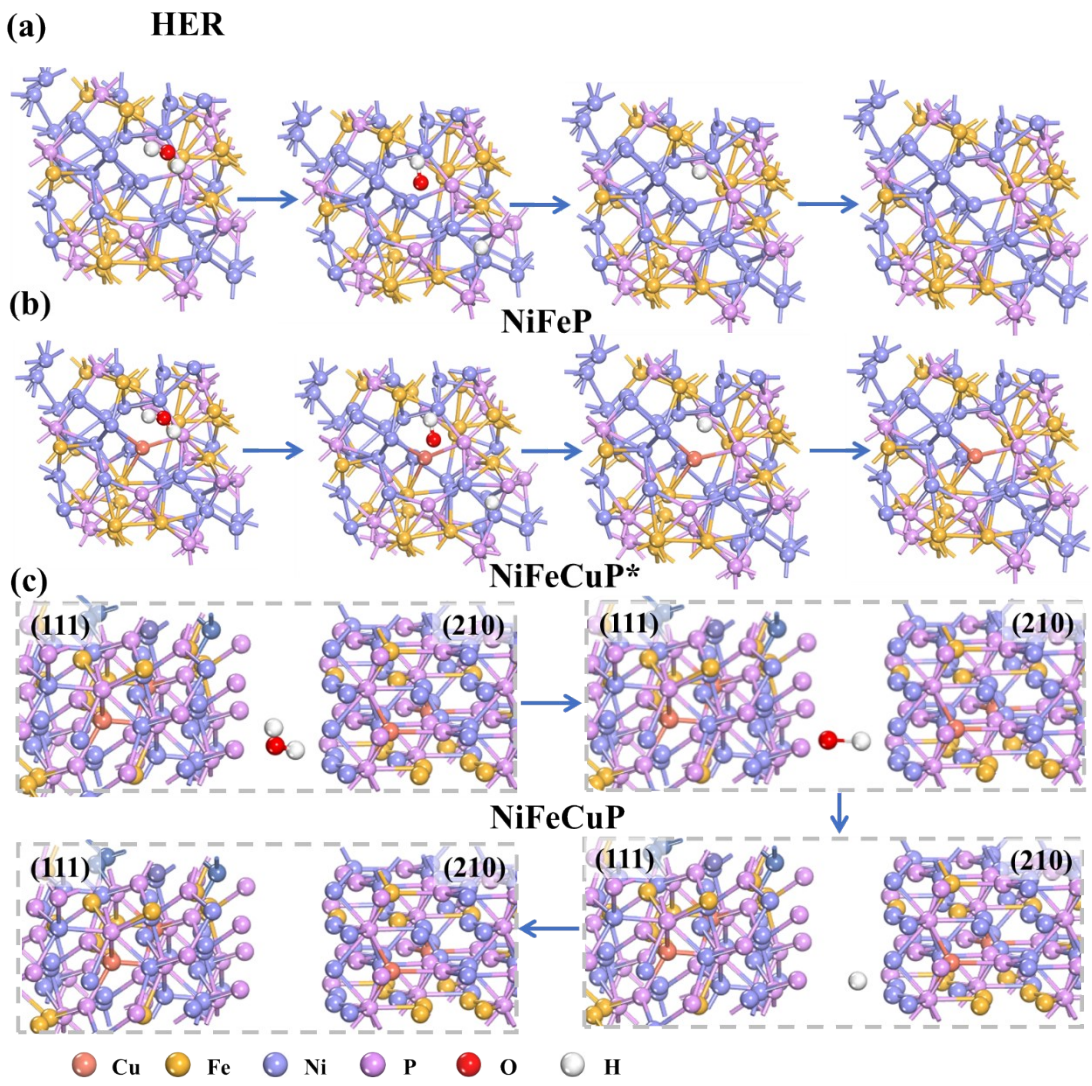

Figure S12. HER reaction pathways and relevant structures of the most possible intermediate steps on the surface of NiFeP and NiFeCuP (NiFeCuP*: the model exposed (111) crystal planes; NiFeCuP: the model exposed (111) and (210) crystal planes).

Table S1. The samples with different Cu contents by ICP-OES test results.

Crystalline	ICP-OES test results		
NiFeCuP-1	Ni 35.94 wt.%	Fe 10.12 wt.%	Cu 0.51 wt.%
NiFeCuP-2	Ni 34.66 wt.%	Fe 9.93 wt.%	Cu 1.08 wt.%
NiFeCuP-3	Ni 33.64 wt.%	Fe 10.06 wt.%	Cu 1.58 wt.%
NiFeCuP-4	Ni 33.01 wt.%	Fe 9.82 wt.%	Cu 2.14 wt.%

Table S2. The samples of NiFeP with different Ni and Fe ratios by ICP-OES test results.

Crystalline	ICP-OES test results	
NiFeP-1	Ni 32.72 wt.%	Fe 14.05 wt.%
NiFeP-2	Ni 33.51 wt.%	Fe 12.92 wt.%
NiFeP-3	Ni 34.34 wt.%	Fe 11.09 wt.%
NiFeP-4	Ni 41.25 wt.%	Fe 7.54 wt.%

By adjusting the addition amount of $Ni(NO_3)_2 \cdot 6H_2O$ and $Fe(NO_3)_3 \cdot 9H_2O$ (The amount of total metal ratios was 12 mmol), the samples with different Ni and Fe ratios were prepared. Based on the Ni and Fe ratios, they are labeled as NiFeP-1, NiFeP-2, NiFeP-3 and NiFeP-4, respectively.

Table S3. Fitting parameters for equivalent circuit model in the electrochemical impedance.

Catalysts	R_1	R_2	CPE-P	CPE-T	R_1	R_2	CPE-P	CPE-T
	HER				OER			
Ni Foam	0.91	112.61	0.86	0.0063	0.99	101.41	0.86	0.0083
NiFeLDH	0.89	9.21	0.89	0.0052	0.91	7.53	0.88	0.011
NiFeCuLDH	0.89	8.17	0.84	1.14	0.91	5.21	0.85	0.011
NiFeP	0.89	5.58	0.73	0.015	0.93	4.69	0.89	0.023
NiFeCuP	0.59	2.78	0.84	0.012	0.81	2.15	0.80	0.008

Notes: R_1 and R_2 are the electrolyte and charge transfer resistance, respectively. CPE is corresponding to the constant phase angle element, which represent double-layer capacitance of solid electrode in the real-world situation.

Table S4. The Gibbs free energy (ΔG) of hydrogen generations and water dissociation during HER and OER on the surface of NiFeP and NiFeCuP, respectively.

	ΔG(H*)/eV	ΔG(H_2O)/eV	ΔG(*OH)/eV	ΔG(*O)/eV	ΔG(*OOH)/eV	ΔG(O_2)/eV
NiFeP	0.65	1.81	0.71	2.15	4.51	4.92
			-0.52	-0.31	0.82	0
NiFeCuP*	0.40	1.65	0.48	1.96	3.87	4.92
			-0.75	-0.5	0.18	0
NiFeCuP	0.35	1.31	0.32	1.83	3.56	4.92
			-0.91	-0.63	-0.13	0

Notes: NiFeCuP* represents the model exposed (111) crystal planes; NiFeCuP represents the model exposed (111) and (210) crystal planes.

Table S5. Summary of several recently representative reported HER electrocatalysts employed in alkaline electrolytes.

Catalysts	J/mA cm^{-2}	Overpotential/mV		Cell voltages/V	References
		HER	OER		
NiFeCuP/NF	10	106	170	1.51	**This work**
NiFeP/SG	10	115	218	1.54	3
CuO@Cu_3P/CF	10	144	267	1.75	4
Co-Cu-P-NS	10	99	272	1.66	5
Mo-NiCoP	10	76	269	1.61	6
NiCoP	10	58	246	1.58	7
Ni_2P/FeP@NG	10	250	295	1.69	8
CoFeP	10	177	350	1.57	9
Fe-CoP	10	79	220	1.55	10
$NC_{0.9}F_{0.1}P$ HHAs/NF	10	122.5	269	1.57	11
NiFeP@N-CS	10	186	216	1.63	12
NiFeP@NiP@NF	10	105	227	1.57	13
CoP@FeCoP/NC	10	141	238	1.68	14
Co_2P/CoP@Co@NCNT	10	118	256	1.60	15
Mo-CoP	10	118	317	1.70	16

NiCoP@PNCNF	10	98	260	1.64	17
NiFeP-CNT@NiCo/CP	10	82	230	1.58	18
CoP-NC@NFP	10	162	270	1.57	19
CC-NC-NiFeP	10	94	145	1.54	20
CoMoP@N, P-C	10	152	296	1.62	21

Reference

1 Y. Huang, Y. Sun, X. Zheng, T. Aoki, B. Pattengale, J. Huang, X. He, W. Bian, S. Younan, N. Williams, J. Hu, J. Ge, N. Pu, X. Yan, X. Pan, L. Zhang, Y. Wei, J. Gu, Atomically engineering activation sites onto metallic 1T-MoS_2 catalysts for enhanced electrochemical hydrogen evolution, *Nat. Commun.*, 2019, **10,** 982.

2 J.M. Zhang, X.P. Xu, L. Yang, D.J. Cheng, D.P. Cao, Single-atom Ru doping induced phase transition of MoS_2 and S vacancy for hydrogen evolution reaction, *Small Methods,* 2019, **3,** 1900653.

3 R.-Q. Li, B.-L. Wang, T. Gao, R. Zhang, C. Xu, X. Jiang, J. Zeng, Y. Bando, P. Hu, Y. Li, X.-B. Wang, Monolithic electrode integrated of ultrathin NiFeP on 3D strutted graphene for bifunctionally efficient overall water splitting, *Nano Energy*, 2019, **58**, 870-876.

4 S. Lv, J. Li, B. Zhang, Y. Shi, X. Liu, T. Wang, In-situ growth of hierarchical CuO@Cu_3P heterostructures with transferable active centers on copper foam substrates as bifunctional electrocatalysts for overall water splitting in alkaline media, *Int. J. Hydrogen Energy,* 2022, **47,** 9593-9605.

5 Y. Liu, Y. Yang, B. Chen, X. Li, M. Guo, Y. Yang, K. Xu, C. Yuan, Highly mesoporous cobalt-hybridized 2D Cu_3P nanosheet arrays as boosting janus electrocatalysts for water splitting, *Inorg. Chem.*, 2021, **60,** 18325-18336.

6 J. Lin, Y. Yan, C. Li, X. Si, H. Wang, J. Qi, J. Cao, Z. Zhong, W. Fei, J. Feng, Bifunctional electrocatalysts based on Mo-doped NiCoP nanosheet arrays for overall water splitting, *Nano-micro Lett.*, 2019, **11,** 55.

7 H. Liang, A.N. Gandi, D.H. Anjum, X. Wang, U. Schwingenschlögl, H.N.

Alshareef, Plasma-assisted synthesis of NiCoP for efficient overall water splitting, *Nano Lett.*, 2016, **16,** 7718-7725.

8 S.H. Yu, Z. Tang, Y. Shao, H. Dai, H.Y. Wang, J. Yan, H. Pan, D.H.C. Chua, In situ hybridizing MoS_2 microflowers on VS_2 microflakes in a one pot CVD Pprocess for electrolytic hydrogen evolution reaction, *ACS Appl. Energy Mater.,* 2019, **2,** 5799-5808.

9 Y. Du, H. Qu, Y. Liu, Y. Han, L. Wang, B. Dong, Bimetallic CoFeP hollow microspheres as highly efficient bifunctional electrocatalysts for overall water splitting in alkaline media, *Appl. Surf. Sci.*, 2019, **465**, 816-823.

10 S. Xu, Y. Qi, Y. Lu, S. Sun, Y. Liu, D. Jiang, Fe-Doped CoP holey nanosheets as bifunctional electrocatalysts for efficient hydrogen and oxygen evolution reactions, *Int. J. Hydrogen Energy,* 2021, **46**, 26391-26401.

11 Y. Qi, Q. Zhang, S. Meng, D. Li, W. Wei, D. Jiang, M. Chen, Iron-doped nickle cobalt ternary phosphide hyperbranched hierarchical arrays for efficient overall water splitting, *Electrochim. Acta*, 2020, **334**, 135633.

12 J. Hei, G. Xu, B. Wei, L. Zhang, H. Ding, D. Liu, NiFeP nanosheets on N-doped carbon sponge as a hierarchically structured bifunctional electrocatalyst for efficient overall water splitting, *Appl. Surf.e Sci.*, 2021, **549,** 149297.

13 F. Diao, W. Huang, G. Ctistis, H. Wackerbarth, Y. Yang, P. Si, J. Zhang, X. Xiao, C. Engelbrekt, Bifunctional and self-supported NiFeP-layer-coated NiP rods for electrochemical water splitting in alkaline solution, *ACS Appl. Mater. Interfaces,* 2021, **13,** 23702-23713.

14 J. Shi, F. Qiu, W. Yuan, M. Guo, Z.-H. Lu, Nitrogen-doped carbon-decorated yolk-shell CoP@FeCoP micro-polyhedra derived from MOF for efficient overall water splitting, *Chem. Eng. J.,* 2021, **403,** 126312.

15 Z. Lu, Y. Cao, J. Xie, J. Hu, K. Wang, D. Jia, Construction of Co_2P/CoP@Co@NCNT rich-interface to synergistically promote overall water splitting, *Chem. Eng. J.,* 2022, **430**, 132877.

16 L. Li, Y. Guo, X. Wang, X. Liu, Y. Lu, Ultraeven Mo-doped CoP nanocrystals as bifunctional electrocatalyst for efficient overall water splitting, *Langmuir*, 2021, **37,** 5986-5992.

17 X. Sun, P. Wei, J. Zhang, S. Gu, R. Yang, C. Fang, Q. Li, J. Han, Z. Jiang, J. He, P, N-codoped carbon nanofibers confined ultra-small bimetallic NiCoP for highly efficient overall water splitting, *Appl. Surf. Sci.*, 2021, **570,** 151247.

18 Z. Wang, C. Wei, X. Zhu, X. Wang, J. He, Y. Zhao, A hierarchical carbon nanotube forest supported metal phosphide electrode for efficient overall water splitting, *J. Mater. Chem. A*, 2021, **9,** 1150-1158.

19 E. Vijayakumar, S. Ramakrishnan, C. Sathiskumar, D.J. Yoo, J. Balamurugan, H.S. Noh, D. Kwon, Y.H. Kim, H. Lee, MOF-derived CoP-nitrogen-doped carbon@NiFeP nanoflakes as an efficient and durable electrocatalyst with multiple catalytically active sites for OER, HER, ORR and rechargeable zinc-air batteries, *Chem. Eng. J.,* 2022, **428,** 131115.

20 J. Bian, Z. Song, X. Li, Y. Zhang, C. Cheng, Nickel iron phosphide ultrathin nanosheets anchored on nitrogen-doped carbon nanoflake arrays as a

bifunctional catalyst for efficient overall water splitting, *Nanoscale*, 2020, **12,** 8443-8452.

21 D. Sun, S. Lin, Y. Yu, S. Liu, F. Meng, G. Du, B. Xu, One-pot synthesis of N and P Co-doped carbon layer stabilized cobalt-doped MoP 3D porous structure for enhanced overall water splitting, *J. Alloys Compd.,* 2022, **895,** 162595.